Article ID: 1000-324X(2019)03-0341-08 **DOI:** 10.15541/jim20180249

Thermoelectric Properties of $(Ag_2Se)_{1-x}(Bi_2Se_3)_x$

LIU Hong-Xia[1,2,3], LI Wen[1], ZHANG Xin-Yue[1], LI Juan[1], PEI Yan-Zhong[1]

(1. Interdisciplinary Materials Research Center, School of Materials Science and Engineering, Tongji University, Shanghai 201804, China; 2. State Key Laboratory of High Performance Ceramics and Superfine Microstructures, Shanghai Institute of Ceramics, Chinese Academy of Sciences, Shanghai 200050, China; 3. University of Chinese Academy of Sciences, Beijing 100049, China)

Abstract: Ternary chalcogenides I-V-VI_2 compounds attract extensive attentions for thermoelectric applications due to their intrinsically low lattice thermal conductivity. $AgBiSe_2$, as one of a few n-type semiconductors among these compounds, shows the potential to be a promising thermoelectric material. Therefore, this work focuses on its thermoelectric properties. According to the phase diagram of Ag_2Se-Bi_2Se_3 system, the single phase region of $(Ag_2Se)_{1-x}(Bi_2Se_3)_x$ allows x to be varied in the range of 0.4~0.62. This large variation of x suggests a tunability of carrier concentration for this material. A broad carrier concentration of 1.0×10^{19}~5.7×10^{19} cm^{-3} for single phased $(Ag_2Se)_{1-x}(Bi_2Se_3)_x$ is obtained through a composition manipulation, which enables a comprehensive assessment on electronic transport properties based on a single parabolic band model with acoustic scattering. The highest carrier concentration obtained in this work, approaching to the theoretical optimal one, leads to a peak ZT of 0.5 at 700 K. This work offers a well understanding of its transport properties and underlying physical parameters determining the thermoelectric performance.

Key words: thermoelectric material; thermoelectric properties; $AgBiSe_2$; carrier concentration; SPB model

Due to the increasingly environmental crisis, development of sustainable clean energy becomes a key challenge in global scientific research[1]. Based on the Seebeck effect, thermoelectrics could directly convert heat into electricity without involving any moving parts and emissions, which has been considered as a solution for the crisis[2-6]. The conversion efficiency of thermoelectric materials mainly depends on the thermoelectric figure of merit, $ZT=S^2T/\rho(k_E+k_L)$, where S, ρ, T, k_E and k_L are the Seebeck coefficient, the electrical resistivity, the absolute temperature, the electronic and lattice thermal conductivities, respectively. Thus, a high S, a low ρ and a low (k_E+k_L) are expected for a superior ZT.

However, the strong coupling among S, ρ and k_E *via* the carrier concentration, band structure and charge scattering, results in a simultaneous optimization of these parameters to be difficult[7-8]. The newly developed strategy of band engineering[9-10] successfully decouples the correlation, leading to a significant enhancement in power factor (S^2/ρ) and then an increased ZT in various materials, such as PbTe[11], SnTe[12-13], GeTe[14-16], SnSe[17], Mg_2Si[18] and half-Heusler[19]. Alternatively, minimizing k_L[20], the only independent parameter determining ZT, through nanostructuring[21-29], point defects[30-34], dislocations[11,35-36], liquid phonons[37-38], low sound velocity[39-41], lattice anharmonicity[42-44], and low cutoff frequency of acoustic phonons[45], has effectively resulted in a ZT-enhancement as well.

Ternary chalcogenides I-V-VI_2 compounds (where I= Cu, Ag or alkali metal; V=Sb, Bi; and VI=S, Se, Te) have aroused widespread interests for thermoelectric applications due to their intrinsically low k_L stemming from the strong anharmonicity induced by lone s^2 pair electrons of the group V cations[46]. So far, the study of their thermoelectric properties mainly focuses on the Ag- based compounds, particularly $Ag(Sb/Bi)(Te/Se)_2$[23,47-55]. The peak ZTs of 2.0 and 1.2 for $AgSbTe_2$ and $AgSbSe_2$ have been realized through band engineering and carrier concentration optimization[48,56], respectively, which are considered as potentially lead-free alternatives for p-type PbTe.

As one of a few n-type semiconductors among this family of compounds, the crystal structure of $AgBiSe_2$ transforms from hexagonal to rhombohedral and then to

Received date: 2018-05-30; **Modified date:** 2018-06-29
Foundation item: National Key Research and Development Program of China (2018YFB0703600); National Natural Science Foundation of China (11474219, 51772215); Fok Ying Tung Education Foundation (20170072210001); Fundamental Research Funds for Shanghai Science and Technology Innovation Plan (18JC1414600); Fundamental Research Funds for the Central Universities
Biography: LIU Hong-Xia (1992–), female, candidate of PhD. E-mail: hongxliu@126.com
Corresponding author: LI Wen, associate professor. E-mail: liwen@tongji.edu.cn

cubic with increasing temperature[57-60], as shown in Fig. 1(a). The cubic $AgBiSe_2$ shows highly disorder at cation sites, which are beneficial for the low k_L through the strong phonon scattering by point defects[61]. Recently, numerous efforts have been put on its thermoelectric performance. In order to enhance the power factor (S^2/ρ), Nb-[52], Ge-[62], In-doping[63] at cation site or Te-[64], Cl-doping[65] at anion site are carried out, and an enhanced ZT up to 0.7 is obtained in single phase $AgBiSe_2$ at 773 K. It is well known that a realization in the highest possible ZT, even using the successful strategies mentioned above, strongly depends on an optimization in carrier concentration[66-68]. Therefore, an investigation on the transport properties in a broad carrier concentration range, is essential to fully assess the potential for thermoelectric applications.

This work focuses on the systematic investigation of the thermoelectric properties of $(Ag_2Se)_{1-x}(Bi_2Se_3)_x$ alloys. A broad carrier concentration ranging from 1.0×10^{19} cm^{-3} to 5.7×10^{19} cm^{-3} is obtained through the control of x, which enables a comprehensive evaluation of the electronic transport properties based on a single parabolic band transport with acoustic scattering. Moreover, the underlying physics including the scattering mechanism, deformation potential coefficient, density-of-states effective mass and optimal carrier concentration are discussed in details. The work offers a fundamental understanding of the transport properties of $(Ag_2Se)_{1-x}(Bi_2Se_3)_x$.

1 Experimental methods

Polycrystalline $(Ag_2Se)_{1-x}(Bi_2Se_3)_x$ ($0.4 \leqslant x \leqslant 0.62$) was synthesized using Ag_2Se and Bi_2Se_3 as the starting materials. Both Ag_2Se and Bi_2Se_3 were synthesized by sealing stoichiometric quantity of Ag (99.999%) and Se (99.999%), Bi (99.999%) and Se (99.999%) in vacuum quartz ampoules, melting at 1273 K and 1123 K for 4 h, respectively, quenching in cold water, and then annealing at 843 K for 3 d. The obtained Ag_2Se and Bi_2Se_3 ingots were weighed according to the stoichiometric ratio, melted at 1173 K for 10 h and annealed at 843 K for 2 d. Pellet samples (>96% of the theoretical density) with ~12.0 mm in diameter were obtained by an induction heating hot press system at 800 K for 30 min under a uniaxial pressure of ~ 80 MPa.

The details of the electronic transports (Seebeck coefficient, electronic resistivity and Hall coefficient) measurements are given in the literature[69]. The thermal conductivity was estimated *via* $\kappa = dC_pD$, where d is the geometric density, C_p is the heat capacity, and D is the thermal diffusivity. Parameter D was measured using a laser flash technique with the Netzsch LFA457 system, and C_p was determined by the Dulong-Petit limit and assumed to be temperature independent. All the transport property measurements were carried out under helium atmosphere from 300 K to 700 K. The measurement uncertainty for each transport property (S, ρ and κ) is about 5%.

Phase composition and microstructures were identified by X-Ray Diffraction (XRD) and Scanning Electron Microscope (SEM, Phenom Pro) equipped with an Energy Dispersive spectrometer. The longitudinal (v_L) and transverse (v_T) sound velocities were measured on the pellet samples at room temperature using an ultrasonic pulse receiver (Olympus-NDT) equipped with an oscilloscope (Keysight). Infrared Fourier transform spectroscopy (Bruker Tensor 2) was used to measure the optical reflectance coefficient for estimating the optical band gap[70].

2 Results and discussion

According to the phase diagram of Ag_2Se-Bi_2Se_3 system[57] (Fig. 1(b)), $(Ag_2Se)_{1-x}(Bi_2Se_3)_x$ shows a single phase region at x ranging from 0.4 to 0.62. This tunable composition in a broad range suggests an availability of carrier concentration tuning for thermoelectric $(Ag_2Se)_{1-x}(Bi_2Se_3)_x$. Powder XRD patterns for $(Ag_2Se)_{1-x}(Bi_2Se_3)_x$ ($0.4\leqslant x\leqslant0.62$) are shown in Fig. 2. It is found that the single phase region confines x to be from 0.48 to 0.56, since Ag_2Se and Bi_2Se_3 impurity phases are observed for the samples with $x\leqslant0.46$ and $x\geqslant0.58$, respectively. As shown in Fig. 3(a),

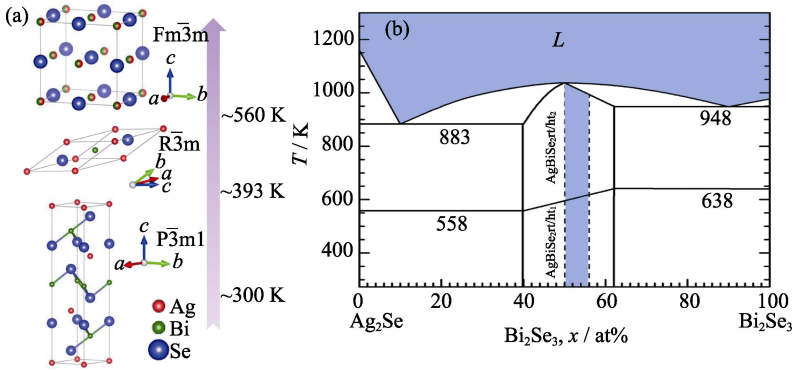

Fig. 1 Crystal structures for the different phases of $AgBiSe_2$ (a) and phase diagram of Ag_2Se-Bi_2Se_3 system (b)[57]

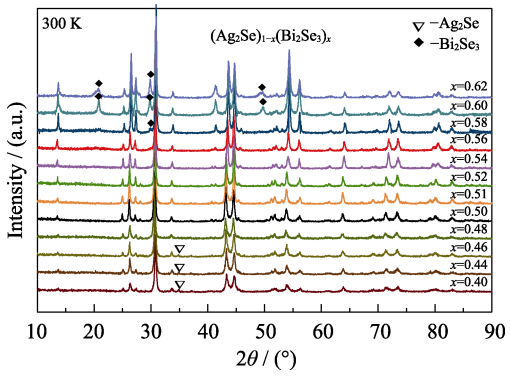

Fig. 2　Powder XRD patterns for $(Ag_2Se)_{1-x}(Bi_2Se_3)_x$ ($0.4 \leqslant x \leqslant 0.62$)

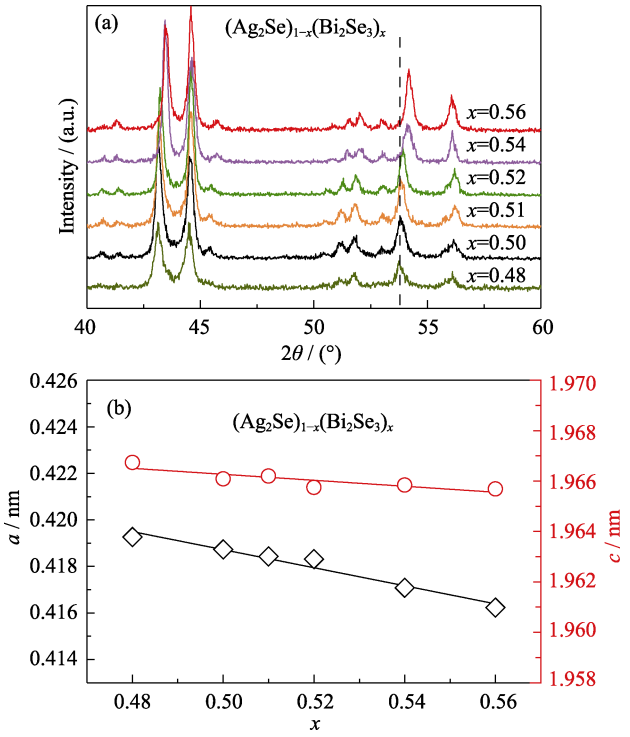

Fig. 3　Locally enlarged XRD patterns (a) and composition dependent lattice parameters (b) for the samples with $0.48 \leqslant x \leqslant 0.56$

the locally enlarged XRD patterns for the samples with single phase ($0.48 \leqslant x \leqslant 0.56$) show that the diffraction peaks shift to higher angles with increasing x. The dependence of lattice parameters on x in Fig. 3(b) shows that both a and c decrease with increasing x, which can be understood by the introduction of cation vacancy as $x>0.5$.

To further confirm the phase purity, the microstructure for the samples with $0.48 \leqslant x \leqslant 0.58$ is characterized by SEM (Fig. 4(a, c-g)), and the mapping on the composition by EDS is carried out on the samples with x=0.48 (Fig. 4(b)) and 0.58 (Fig. 4(h)). No impurity phase can be observed for the samples with $0.5 \leqslant x \leqslant 0.56$. Two types of precipitate are observed in the sample with x=0.48, as shown in Fig. 4(a). The EDS mappings (Fig. 4(b)) show black and white precipitates which are mainly composed of Ag-Se and Bi, respectively. The ratios of Ag:Bi:Se are about 60.1 : 9.3 : 30.6 and 8.9 : 84 : 7.1, respectively, which suggest Ag_2Se and Bi impurities. Moreover, Bi_2Se_3-rich precipitates identified by EDS as well, are observed in the sample 0.58, respectively. Both XRD and SEM results suggest the single phase $(Ag_2Se)_{1-x}(Bi_2Se_3)_x$ region of x being 0.5–0.56. Therefore, single phased $(Ag_2Se)_{1-x}(Bi_2Se_3)_x$ materials with $0.5 \leqslant x \leqslant 0.56$ are focused on.

As shown in Fig. 5(a), the Hall carrier concentration (n_H) for $(Ag_2Se)_{1-x}(Bi_2Se_3)_x$ is found to significantly increase with increasing x. It can be understood by the increase of x would lead to the formation of cation vacancies, which further drives the evaporation of Se due to its high vapor pressure. The deficiency of Se anions would lead to an increase in electron concentration. As a result, an increase in carrier concentration from 1.0×10^{19} cm^{-3} to 5.7×10^{19} cm^{-3} is obtained with increasing x from 0.5 to 0.56. Such a broad carrier concentration range enables a detailed assessment on the electronic transport properties, and a comprehensive understanding of fundamental material parameters. The optical measurements for all the samples are shown in Fig. 5(b). The estimated optical band gap (E_g) is about 0.45 eV, which is in good agreement with literatures (0.5–0.6 eV)[65,71].

Temperature dependent Hall coefficient (R_H) and Hall mobility (μ_H) for $(Ag_2Se)_{1-x}(Bi_2Se_3)_x$ are shown in Fig. 6(a). A sharp decrease in μ_H and R_H around 550 K are found, which can reasonably be attributed to the phase transition between rhombohedral and cubic structures. At temperatures apart from phase transition temperature, R_H in three phases keeps nearly temperature independent, suggesting a single band transport behavior in a degenerated state. The decrease in μ_H with increasing temperature *via* $\mu_H \sim T^{-1.5}$, indicates the charge carrier scattering by acoustic phonons.

According to the above discussion on R_H, a single parabolic band model with acoustic phonon scattering is used to understand the transport properties and underlying physical parameters. Assuming a single band valley (band degeneracy of 2), temperature dependent effective deformation potential coefficient (E_{def}) and density of state effective mass (m^*) are shown in Fig. 6(b). It is found that the changes of both carrier concentration and temperature have negligible effects on both E_{def} and m^* for the samples in three phases, indicating a rigid band behavior for $(Ag_2Se)_{1-x}(Bi_2Se_3)_x$. An m^* of ~0.51 m_e and a E_{def} of ~33 eV are obtained for the samples in the hexagonal structure. The obtained m^* is in good agreement with literature [65]. m^* and E_{def} in the rhombohedral phase are about 0.54 m_e and 29 eV, respectively, while about 4 m_e and 10 eV in the cubic phase.

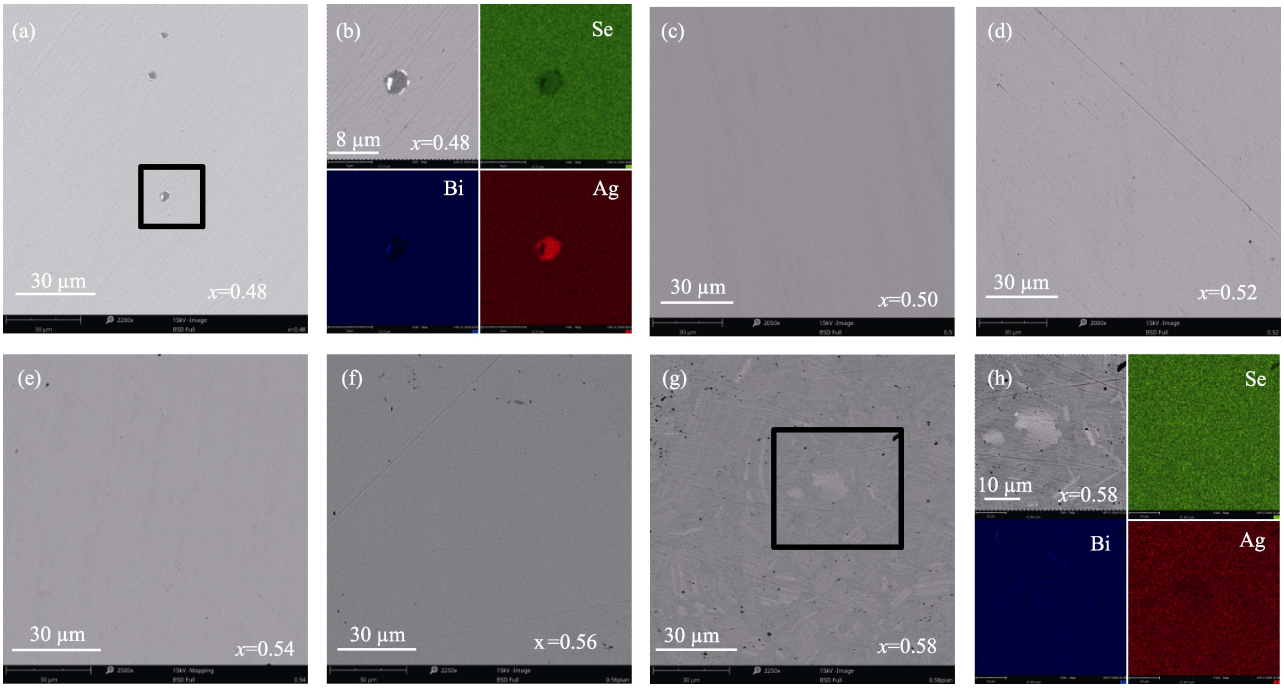

Fig. 4 SEM images for $(Ag_2Se)_{1-x}(Bi_2Se_3)_x$ ($0.48 \leqslant x \leqslant 0.56$) (a, c-g) and its corresponding EDS mapping for the samples with x=0.48 (b) and 0.58 (h)

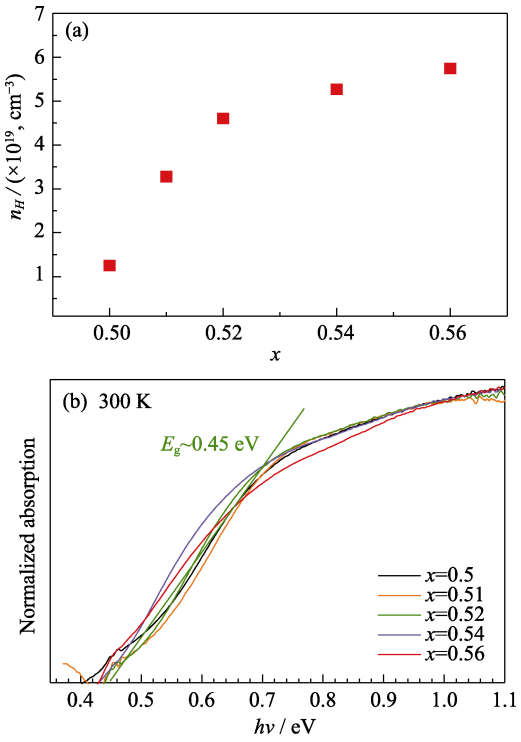

Fig. 5 Composition dependent Hall carrier concentration (a) and normalized optical absorption *versus* photon energy (b) at room temperature for $(Ag_2Se)_{1-x}(Bi_2Se_3)_x$ ($0.5 \leqslant x \leqslant 0.56$)

The Hall carrier concentration dependent Hall mobility, and Seebeck coefficient are shown in Fig. 6(c, d) respectively. Based on estimated average m^* and E_{def} at each temperature (in Fig. 6(b)), the SPB model with the acoustic phonon scattering enables a reasonable prediction on both Seebeck coefficient and Hall mobility at three different temperatures. Moreover, this model prediction agrees well with available literature results[52,64-65].

Temperature dependent Seebeck coefficient and electrical resistivity for $(Ag_2Se)_{1-x}(Bi_2Se_3)_x$ are shown in Fig. 7(a, b), respectively. Both Seebeck coefficient and electrical resistivity decrease with increasing x due to the increase of Hall carrier concentration. Moreover, both of them increase with increasing temperature, showing a degenerate semiconducting behavior. Figure 7(a, b) also include the Seebeck coefficient and electrical resistivity for pristine[64] and In-doped[63] $AgBiSe_2$ from literatures for comparison, respectively. It is seen that the lowest Seebeck coefficient and electrical resistivity obtained in this work is comparable to those of In-doped sample. The Seebeck coefficient for all the samples is negative, indicating a n-type conduction, which is consistent with the Hall coefficient measurements (Fig. 6(a)).

Figure 7(c, d) show the temperature dependent total thermal conductivity (κ) and lattice thermal conductivity (κ_L) for $(Ag_2Se)_{1-x}(Bi_2Se_3)_x$, respectively. κ_L is obtained by subtracting the electronic thermal conductivity (κ_E) from the total thermal conductivity *via* the Wiedemann-Franz Law, $\kappa_E = LT/\rho$, where L is the Lorenz factor determined by the SPB model with the acoustic phonon scattering. Both κ and κ_L decrease with increasing temperature. The κ slightly increase with increasing x due to the increased carrier concentration leading to higher κ_E. It is seen that the κ_L is lower than 0.7 W/(m·K) in the entire temperature range, mainly resulting from the strong anharmonicity[42,46,72] and strong phonon scattering by

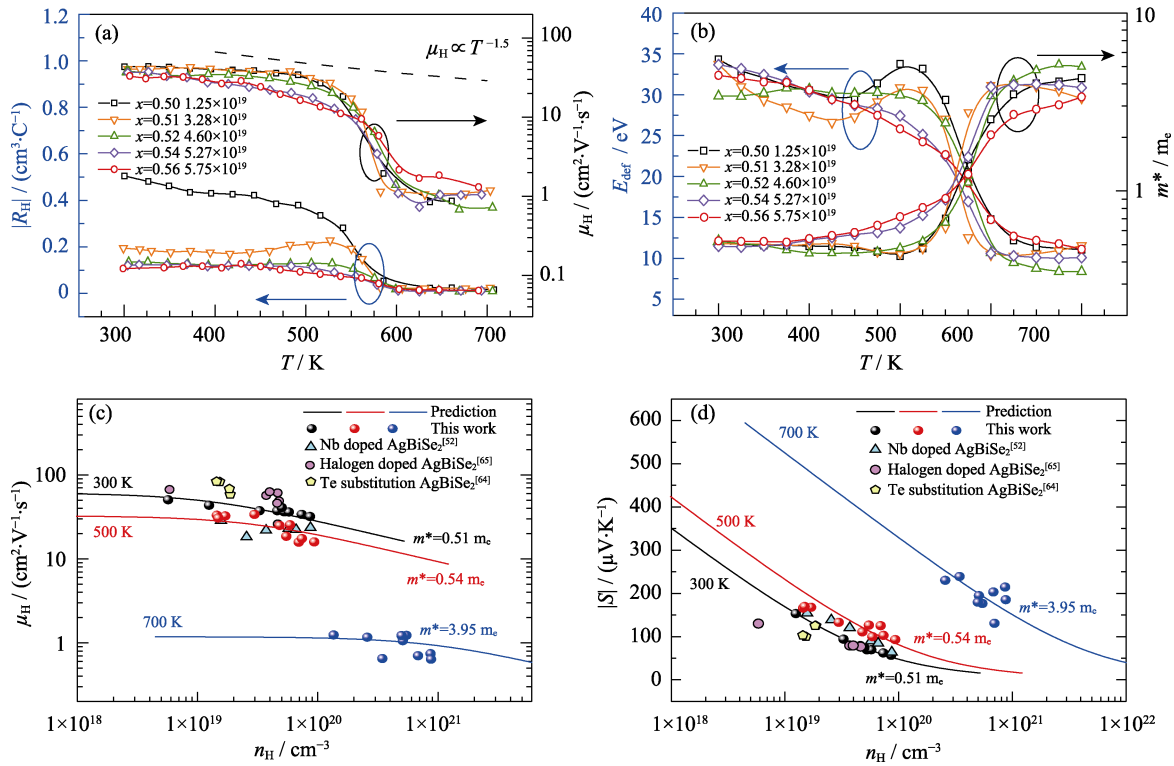

Fig. 6　Temperature dependent Hall coefficient (R_H) and mobility (μ_H) (a), deformation potential coefficient (E_{def}) and density of states effective mass (m^*) (b), Hall carrier concentration dependent Hall mobility (c) and Seebeck coefficient (d) at different temperatures for $(Ag_2Se)_{1-x}(Bi_2Se_3)_x$ ($0.5 \leqslant x \leqslant 0.56$), with a comparison to available literature results[52,64-65].
The experimental results here agree well with the model prediction based on a SPB approximation with a dominant scattering by acoustic phonons

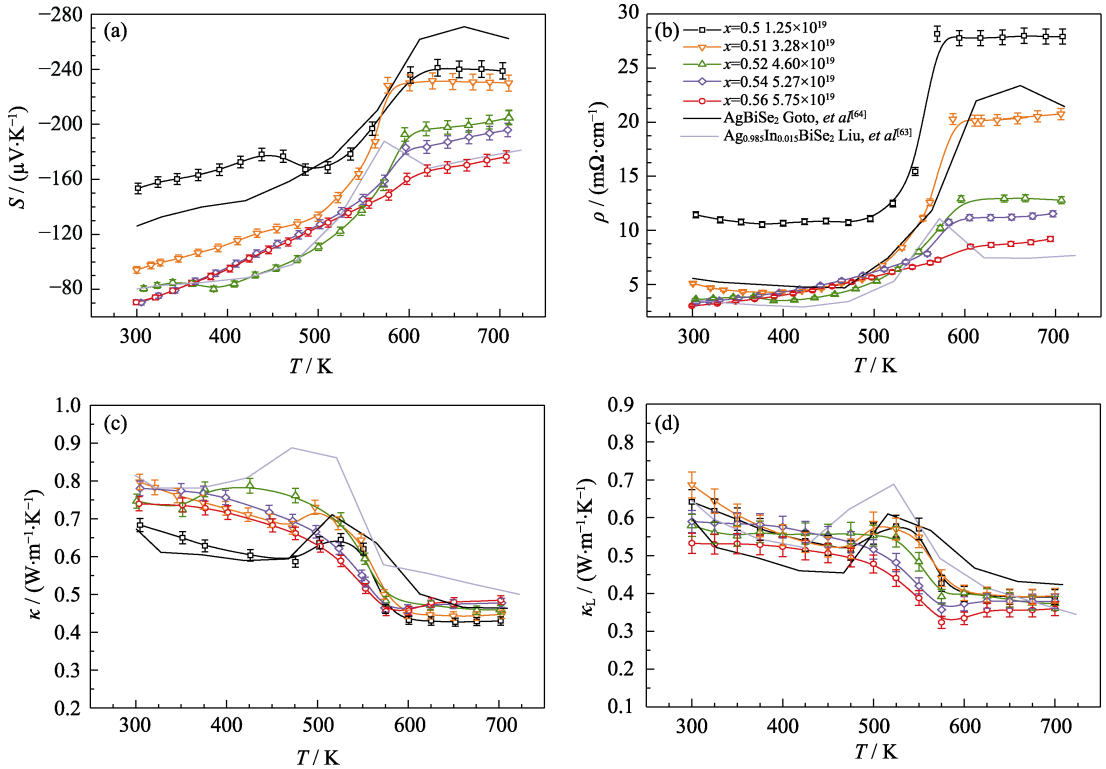

Fig. 7　Temperature dependent Seebeck coefficient (a), electrical resistivity (b), total thermal conductivity (c) and lattice thermal conductivity (d) for $(Ag_2Se)_{1-x}(Bi_2Se_3)_x$ ($0.5 \leqslant x \leqslant 0.56$), with a comparison to available literature results[63-64]

disorded cations[42,61,72]. The κ_L at high temperatures in the cubic phase is found to be as low as~0.4 W/(m·K), showing great potential for thermoelectric applications.

The sound velocities (v_s) of longitudinal (v_L) and

transverse (v_T) branches, as the important parameters determining κ_L, are measured and listed in Table 1. Moreover, the physical parameters including Debye temperature (θ_D), bulk modulus (B) and Grüeneisen parameter (γ) are estimated based on the measured v_L and v_T[73-74], as listed in Table 1. It is shown that the change in sound velocities for all the samples does not exceed 5%, which is within the measurement uncertainty range. This excludes the influence of lattice softening on κ_L. This material shows a very low sound velocity of ~1500 m/s, one of the lowest sound velocities among thermoelectrics[39,75]. Moreover, the Grüneisen parameter (γ) as large as 2 indicates the strong anharmonicity[46]. Both the low sound velocity and the strong lattice anharmonicity could be the origin for the low κ_L observed.

Temperature dependent figure of merit (ZT) for $(Ag_2Se)_{1-x}(Bi_2Se_3)_x$ is shown in Fig. 8(a). ZTs for all the samples increase with increasing temperature and x, due to the carrier concentration optimization. Thus, a peak ZT of 0.5 at 700 K is achieved for the sample with the highest carrier concentration. The SPB model further enables a prediction in carrier concentration dependent ZT at different temperatures using the experimental κ_L (Fig. 8(b)). The predicted ZT agrees well with the experimental data as shown in Fig. 8(b). It is found the highest carrier concentration obtained in this work is very close to the optimal one. According to the calculated band structure[71], engineering the band should enable a possibility for further enhancing the thermoelectric performance.

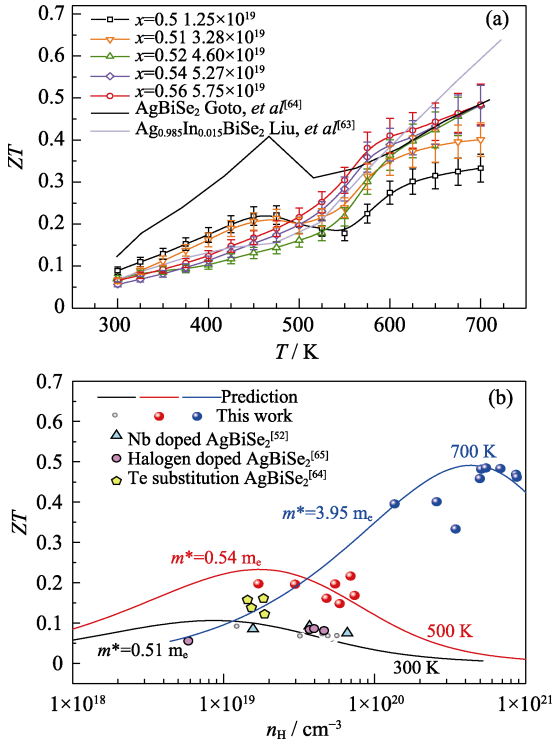

Fig. 8 Temperature dependent ZT for $(Ag_2Se)_{1-x}(Bi_2Se_3)_x$ ($0.5 \leqslant x \leqslant 0.56$) (a) and Hall carrier concentration dependent ZT at different temperatures (b) with a comparison to model prediction and literature results[52,63-65]

3 Conclusion

In this work, a composition control for $(Ag_2Se)_{1-x}(Bi_2Se_3)_x$ with x in the range of 0.5–0.56 enables the carrier concentration ranging in $(1.0–5.7)\times10^{19}$ cm^{-3}, which allows a systematical understanding on the fundamental physical parameters determining its transport properties. It is shown that the electronic transport properties can be well understood by a single parabolic band model. The carrier concentration is well optimized in this work, leading to a peak ZT of 0.5 with the help of intrinsically low lattice thermal conductivity. This work offers a fundamental understanding on the material physics affecting the thermoelectric performance, which could guide the further improvements for this material.

Table 1 Measured sound velocities and the estimated physical parameters for $(Ag_2Se)_{1-x}(Bi_2Se_3)_x$ ($0.5 \leqslant x \leqslant 0.56$)

$(Ag_2Se)_{1-x}(Bi_2Se_3)_x$	v_T/ (m·s^{-1})	v_L/ (m·s^{-1})	v_s/ (m·s^{-1})	B/ GPa	γ	θ_D /K
x=0.5	1390	2560	1550	31.5	1.7	158
x=0.51	1410	2610	1570	32.4	1.7	159
x=0.52	1360	2500	1520	29.6	1.7	154
x=0.54	1290	2660	1450	37.8	2.1	146
x=0.56	1380	2760	1550	39.8	2.0	156

References

[1] XI H, LUO L, FRAISSE G. Development and applications of solar-based thermoelectric technologies. *Renewable and Sustainable Energy Reviews*, 2007, **11(5):** 923–936.

[2] HAMID ELSHEIKH M, SHNAWAH D A, SABRI M F M, *et al*. A review on thermoelectric renewable energy: principle parameters that affect their performance. *Renewable and Sustainable Energy Reviews*, 2014, **30:** 337–355.

[3] CADOFF I B, MILLER E. Thermoelectric materials and devices, New York: Reinhold Pub. Corp., 1960: p xiii, 344p.

[4] BELL L E. Cooling, heating, generating power, and recovering waste heat with thermoelectric systems. *Science*, 2008, **321(5895):** 1457–1461.

[5] TRITT T M. Recent Trends in Thermoelectric Materials Research. San Diego: Academic Press, 2001.

[6] WOOD C. Materials for thermoelectric energy conversion. *Reports on Progress in Physics*, 1988, **51(4):** 459–539.

[7] SNYDER G J, TOBERER E S. Complex thermoelectric materials. *Nature Materials*, 2008, **7(2):** 105–114.

[8] BHANDARI C M, ROWE D M. Thermoelectric Transport Theory. In CRC handbook of thermoelectrics, Rowe, D. M., Ed. Boca Raton: CRC Press, 1995: 27–42.

[9] PEI Y, SHI X, LALONDE A, *et al*. Convergence of electronic bands for high performance bulk thermoelectrics. *Nature*, 2011, **473(7345):** 66–69.

[10] LIN S, LI W, CHEN Z, *et al*. Tellurium as a high-performance elemental thermoelectric. *Nature Communications*, 2016, **7:** 10287.

[11] CHEN Z, JIAN Z, LI W, *et al*. Lattice dislocations enhancing thermoelectric PbTe in addition to band convergence. *Advanced Materials*, 2017, **29(23):** 1606768.

[12] LI W, WU Y, LIN S, *et al*. Advances in environment-friendly SnTe thermoelectrics. *ACS Energy Letters*, 2017, **2(10):** 2349–2355.

[13] LI W, ZHENG L L, GE B H, *et al*. Promoting SnTe as an eco-friendly solution for p-PbTe thermoelectric *via* band convergence and interstitial defects. *Advanced Materials*, 2017, **29(17):** 1605887–1–8.

[14] LI J, ZHANG X, CHEN Z, *et al*. Low-symmetry rhombohedral GeTe thermoelectrics. *Joule*, 2018, **2(5):** 976–987.

[15] LI J, CHEN Z, ZHANG X, *et al*. Simultaneous optimization of carrier concentration and alloy scattering for ultrahigh performance GeTe thermoelectrics. *Advanced Science*, 2017, **4(12):** 1700341–1–9.

[16] HONG M, CHEN Z G, YANG L, *et al*. Realizing *zT* of 2.3 in $Ge_{1-x-y}Sb_xIn_yTe$ *via* reducing the phase-transition temperature and introducing resonant energy doping. *Advanced Materials*, 2018, **30(11):** 1705942–1–8.

[17] HONG A J, LI L, ZHU H X, *et al*. Optimizing the thermoelectric performance of low-temperature SnSe compounds by electronic structure design. *Journal of Materials Chemistry A*, 2015, **3(25):** 13365–13370.

[18] LIU W, TAN X, YIN K, *et al*. Convergence of conduction bands as a means of enhancing thermoelectric performance of n-type $Mg_2Si_{1-x}Sn_x$ solid solutions. *Phys. Rev. Lett.*, 2012, **108(16):** 166601.

[19] FU C G, BAI S Q, LIU Y T, *et al*. Realizing high figure of merit in heavy-band p-type half-Heusler thermoelectric materials. *Nat. Commun.*, 2015, **6:** 8144–1–7.

[20] CHEN Z, ZHANG X, PEI Y. Manipulation of phonon transport in thermoelectrics. *Advanced Materials*, 2018, **2(1):** 1705617–1–12.

[21] KANATZIDIS M G. Nanostructured thermoelectrics: the new paradigm? *Chemistry of Materials*, 2010, **22(3):** 648–659.

[22] PEI Y Z, LENSCH-FALK J, TOBERER E S, *et al*. High thermoelectric performance in PbTe due to large nanoscale Ag_2Te precipitates and La doping. *Advanced Functional Materials*, 2011, **21(2):** 241–249.

[23] XU J J, LI H, DU B L, *et al*. High *ZT* in nanostructuring $AgSbTe_2$. *Journal of Materials Chemistry*, 2010, **20(29):** 6138–6143.

[24] SCHAUMANN J, LOOR M, UNAL D, *et al*. Improving the *zT* value of thermoelectrics by nanostructuring: tuning the nanoparticle morphology of Sb_2Te_3 by using ionic liquids. *Dalton Trans*, 2017, **46(3):** 656–668.

[25] PICHANUSAKORN P, BANDARU P. Nanostructured thermoelectrics. *Materials Science and Engineering*: *R: Reports*, 2010, **67(2/3/4):** 19–63.

[26] ZOU T, QIN X, ZHANG Y, *et al*. Enhanced thermoelectric performance of beta-Zn_4Sb_3 based nanocomposites through combined effects of density of states resonance and carrier energy filtering. *Scientific Reports*, 2015, **5:** 17803–1–9.

[27] POUDEL B, HAO Q, MA Y, *et al*. High-thermoelectric performance of nanostructured bismuth antimony telluride bulk alloys. *Science*, 2008, **320(5876):** 634–638.

[28] HONG M, CHEN Z G, YANG L, *et al*. $Bi_xSb_{2-x}Te_3$ nanoplates with enhanced thermoelectric performance due to sufficiently decoupled electronic transport properties and strong wide-frequency phonon scatterings. *Nano Energy*, 2016, **20:** 144–155.

[29] HONG M, CHASAPIS T C, CHEN Z G, *et al*. n-type $Bi_2Te_{3-x}Se_x$ nanoplates with enhanced thermoelectric efficiency driven by wide-frequency phonon scatterings and synergistic carrier scatterings. *ACS Nano*, 2016, **10(4):** 4719–4727.

[30] LI W, LIN S, ZHANG X, *et al*. Thermoelectric properties of Cu_2SnSe_4 with intrinsic vacancy. *Chemistry of Materials*, 2016, **28(17):** 6227–6232.

[31] HU L, ZHU T, LIU X, *et al*. Point defect engineering of high-performance bismuth-telluride-based thermoelectric materials. *Advanced Functional Materials*, 2014, **24(33):** 5211–5218.

[32] PEI Y, ZHENG L, LI W, *et al*. Interstitial point defect scattering contributing to high thermoelectric performance in SnTe. *Advanced Electronic Materials*, 2016, **2(6):** 1600019.

[33] SHEN J W, ZHANG X Y, CHEN Z W, *et al*. Substitutional defects enhancing thermoelectric $CuGaTe_2$. *Journal of Materials Chemistry A*, 2017, **5(11):** 5314–5320.

[34] BOZHKO V V, NOVOSAD O V, PARASYUK O V, *et al*. Influence of cation-vacancy defects on the properties of $CuInSe_2$-$ZnIn_2Se_4$ solid solutions. *Journal of Alloys and Compounds*, 2015, **618:** 712–717.

[35] KIM S I, LEE K H, MUN H A, *et al*. Thermoelectrics dense dislocation arrays embedded in grain boundaries for high-performance bulk thermoelectrics. *Science*, 2015, **348(6230):** 109–114.

[36] CHEN Z, GE B, LI W, *et al*. Vacancy-induced dislocations within grains for high-performance PbSe thermoelectrics. *Nat. Commun.*, 2017, **8:** 13828–1–8.

[37] LIU H, SHI X, XU F, *et al*. Copper ion liquid-like thermoelectrics. *Nat. Mater.*, 2012, **11(5):** 422–425.

[38] QIU W, XI L, WEI P, *et al*. Part-crystalline part-liquid state and rattling-like thermal damping in materials with chemical-bond hierarchy. *PNAS*, 2014, **111(42):** 15031–15035.

[39] LI W, LIN S, GE B, *et al*. Low sound velocity contributing to the high thermoelectric performance of Ag_8SnSe_6. *Advanced Science*, 2016, **3(11):** 1600196–1–7.

[40] ZHANG X, CHEN Z, LIN S, *et al*. Promising thermoelectric $Ag_{5-\delta}Te_3$ with intrinsic low lattice thermal conductivity. *ACS Energy Letters*, 2017, **2(10):** 2470–2477.

[41] LI WEN, LIN SIQI, WEISS MANUEL, *et al*. Crystal structure induced ultralow lattice thermal conductivity in thermoelectric Ag_9AlSe_6. *Advanced Energy Materials*, 2018, **8:** 1800030–1–8.

[42] MORELLI D T, JOVOVIC V, HEREMANS J P. Intrinsically minimal thermal conductivity in cubic I-V-VI_2 semiconductors. *Phys. Rev. Lett.*, 2008, **101(3):** 035901–1–4.

[43] GUIN S N, NEGI D S, DATTA R, *et al*. Nanostructuring, carrier engineering and bond anharmonicity synergistically boost the thermoelectric performance of p-type $AgSbSe_2$-ZnSe. *Journal of Materials Chemistry A*, 2014, **2(12):** 4324–4331.

[44] HONG A J, GONG J J, LI L, *et al*. Predicting high thermoelectric performance of ABX ternary compounds NaMgX (X = P, Sb, As) with weak electron-phonon coupling and strong bonding anharmonicity. *J. Mater. Chem. C*, 2016, **4(15):** 3281–3289.

[45] LIN S, LI W, LI S, *et al*. High thermoelectric performance of Ag_9GaSe_6 enabled by low cutoff frequency of acoustic phonons. *Joule*, 2017, **1(4):** 816–830.

[46] NIELSEN M D, OZOLINS V, HEREMANS J P. Lone pair electrons minimize lattice thermal conductivity. *Energy Environ. Sci.*, 2013, **6(2):** 570–578.

[47] MA J, DELAIRE O, MAY A F, *et al*. Glass-like phonon scattering from a spontaneous nanostructure in $AgSbTe_2$. *Nat. Nano*, 2013, **8(6):** 445–451.

[48] LI D, QIN X Y, ZOU T H, *et al*. High thermoelectric properties for Sn-doped $AgSbSe_2$. *Journal of Alloys and Compounds*, 2015, **635:** 87–91.

[49] GUIN S N, CHATTERJEE A, NEGI D S, *et al*. High thermoelectric performance in tellurium free p-type $AgSbSe_2$. *Energy & Environmental Science*, 2013, **6(9):** 2603–2608.

[50] GUIN S N, CHATTERJEE A, BISWAS K. Enhanced thermoelec-

tric performance in p-type $AgSbSe_2$ by Cd-doping. *RSC Advances*, 2014, **4(23):** 11811–11815.
[51] CAI S, LIU Z, SUN J, *et al*. Enhancement of thermoelectric properties by Na doping in Te-free p-type $AgSbSe_2$. *Dalton Trans*, 2015, **44(3):** 1046–1051.
[52] PAN L, BERARDAN D, DRAGOE N. High thermoelectric properties of n-type $AgBiSe_2$. *J. Am. Chem. Soc.*, 2013, **135(13):** 4914–4917.
[53] ZOU M, LIU Q, WU C F, *et al*. Comparing the role of annealing on the transport properties of polymorphous $AgBiSe_2$ and monophase $AgSbSe_2$. *RSC Advances*, 2018, **8(13):** 7055–7061.
[54] XIAO C, QIN X, ZHANG J, *et al*. High thermoelectric and reversible p-n-p conduction type switching integrated in dimetal chalcogenide. *J. Am. Chem. Soc.*, 2012, **134(44):** 18460–18466.
[55] GAO W, WANG Z, HUANG J, *et al*. Extraordinary thermoelectric performance realized in hierarchically structured $AgSbSe_2$ with ultralow thermal conductivity. *ACS Appl. Mater. Interfaces*, 2018, **10(22):** 18685–18692.
[56] HONG M, CHEN Z G, YANG L, *et al*. Achieving *ZT*>2 in p-type $AgSbTe_{2-x}Se_x$ alloys *via* exploring the extra light valence band and introducing dense stacking faults. *Advanced Energy Materials*, 2018, **8(9):** 1702333–1–7.
[57] TADAMASA H, KAZUHIRO K, MOTOHISA H. Phase diagrams of the pseudo-binary Cu_2Se-Bi_2Se_3 and Ag_2Se-Bi_2Se_3 systems and thermoelectric properties of Cu_2Se-Bi_2Se_3 solid solution. *Advanced Energy Conversion*, 1966, **6(4):** 195–200.
[58] WERNICK J H, GELLER S, BENSON K E. Constitution of the $AgSbSe_2$-$AgSbTe_2$-$AgBiSe_2$-$AgBiTe_2$ system. *Journal of Physics & Chemistry of Solids*, 1958, **7(2):** 240–248.
[59] MANOLIKAS C, SPYRIDELIS J. Electron microscopic study of polymorphismand defects in $AgBiSe_2$ and $AgBiS_2$. *Mat. Res. Bull.*, 1977, **12:** 907–913.
[60] GELLER S, WERNICK J H. Ternary semiconducting compounds with sodium chloride-like structure-$AgSbSe_2$, $AgSbTe_2$, $AgBiS_2$, $AgBiSe_2$. *Inorganic Chemistry*, 2001, **20(7):** 2246–2250.
[61] HOANG K, MAHANTI S D. Atomic and electronic structures of I-V-VI_2 ternary chalcogenides. *Journal of Science: Advanced Materials and Devices*, 2016, **1(1):** 51–56.
[62] WU H J, WEI P C, CHENG H Y, *et al*. Ultralow thermal conductivity in n-type Ge-doped $AgBiSe_2$ thermoelectric materials. *Acta Materialia*, 2017, **141:** 217–229.
[63] LIU X C, JIN D, LIANG X. Enhanced thermoelectric performance of n-type transformable $AgBiSe_2$ polymorphs by indium doping. *Applied Physics Letters*, 2016, **109(13):** 133901–1–5.
[64] GOTO Y, NISHIDA A, NISHIATE H, *et al*. Effect of Te substitution on crystal structure and transport properties of $AgBiSe_2$ thermoelectric material. *Dalton Trans.*, 2018, **47(8):** 2575–2580.
[65] GUIN S N, SRIHARI V, BISWAS K. Promising thermoelectric performance in n-type $AgBiSe_2$: effect of aliovalent anion doping. *Journal of Materials Chemistry A*, 2015, **3(2):** 648–655.
[66] BHANDARI C M, ROWE D M. Optimization of Carrier Concentration. In CRC Handbook of Thermoelectrics, Rowe, D. M., Ed. Boca Raton: CRC Press, 1995**:** 43–53.
[67] PEI Y Z, GIBBS Z M, GLOSKOVSKII A, *et al*. Optimum carrier concentration in n-type PbTe thermoelectrics. *Advanced Energy Materials*, 2014, **4(13):** 1400486–1–12.
[68] ZHANG X Y, PEI Y Z. Manipulation of charge transport in thermoelectrics. *npj Quantum Materials*, 2017, **2:** 68–1–5.
[69] LI W, CHEN Z, LIN S, *et al*. Band and scattering tuning for high performance thermoelectric $Sn_{1-x}Mn_xTe$ alloys. *Journal of Materiomics*, 2015, **1(4):** 307–315.
[70] GIBBS Z M, LALONDE A, SNYDER G J. Optical band gap and the Burstein-Moss effect in iodine doped PbTe using diffuse reflectance infrared Fourier transform spectroscopy. *New Journal of Physics*, 2013, **15(7):** 075020–1–18.
[71] PARKER D S, MAY A F, SINGH D J. Benefits of carrier-pocket anisotropy to thermoelectric performance: the case of p-type $AgBiSe_2$. *Physical Review Applied*, 2015, **3(6):** 064003–1–11.
[72] BOCHER F, CULVER S P, PEILSTOCKER J, *et al*. Vacancy and anti-site disorder scattering in $AgBiSe_2$ thermoelectrics. *Dalton Trans*, 2017, **46(12):** 3906–3914.
[73] ROUFOSSE M, KLEMENS P G. Thermal conductivity of complex dielectric crystals. *Physical Review B*, 1973, **7(12):** 5379–5386.
[74] SANDITOV D S, BELOMESTNYKH V N. Relation between the parameters of the elasticity theory and averaged bulk modulus of solids. *Technical Physics*, 2011, **56(11):** 1619–1623.
[75] BHARDWAJ A, RAJPUT A, SHUKLA A K, *et al*. Mg_3Sb_2-based Zintl compound: a non-toxic, inexpensive and abundant thermoelectric material for power generation. *RSC Advances*, 2013, **3:** 8504–8516.

$(Ag_2Se)_{1-x}(Bi_2Se_3)_x$ 的热电性能研究

刘虹霞[1,2,3], 李 文[1], 张馨月[1], 李 娟[1], 裴艳中[1]

(1. 同济大学 材料科学与工程学院, 材料交叉学科研究中心, 上海 201804; 2. 中国科学院 上海硅酸盐研究所, 高性能陶瓷与超微结构国家重点实验室, 上海 200050; 3. 中国科学院大学, 北京 100049)

摘 要: 具有本征低晶格热导率的 I-V-VI_2 族三元硫属化合物在热电领域引起了广泛关注。$AgBiSe_2$ 作为这类化合物中少有的 n 型半导体, 成为一种有潜力的热电材料。本工作系统研究了 $AgBiSe_2$ 的热电性能。基于 Ag_2Se-Bi_2Se 二元相图, 单相的$(Ag_2Se)_{1-x}(Bi_2Se_3)_x$ 的成分在 x=0.4~0.62 范围可调, 使得该材料载流子浓度具有可调性。结果表明, 通过组分调控获得了较宽范围的载体浓度 1.0×10^{19}~5.7×10^{19} cm^{-3}, 并基于声学声子散射的单一抛物带模型对其电传输性能进行了综合评估。本研究获得的最高载流子浓度接近理论最优值, 在 700 K 实现了最高 *ZT* 值 0.5。本研究有助于深入理解 $AgBiSe_2$ 的传输特性和决定热电性能的基本物理参数。

关 键 词: 热电材料; 热电性能; $AgBiSe_2$; 载流子浓度; SPB 模型

中图分类号: TB34 **文献标识码:** A